Quaternary International 455 (2017) 93–101

Contents lists available at ScienceDirect

Quaternary International

journal homepage: www.elsevier.com/locate/quaint

Downwasting of the debris-covered area of Lirung Glacier in Langtang Valley, Nepal Himalaya, from 1974 to 2010

Takayuki Nuimura*, Koji Fujita, Akiko Sakai

Graduate School of Environmental Studies, Nagoya University, Nagoya, Japan

A R T I C L E I N F O

Article history:
Received 31 October 2016
Received in revised form
14 June 2017
Accepted 29 June 2017
Available online 5 July 2017

A B S T R A C T

Despite the widespread shrinkage of debris-covered Himalayan glaciers in recent decades, the underlying processes driving these changes are poorly understood. This study presents recent mass-balance data for the debris-covered area of Lirung Glacier in Langtang Valley, Nepal Himalaya, constrained using multi-temporal, remotely sensed digital elevation models calibrated to in situ GPS survey data, and surface-flow velocity data from phase-only correlation. The results indicate surface lowering of between −1.3 and −1.8 m a−1 during the study period (1974–2010), with accelerated glacier thinning after 2000. Similarly, we observed a decline in emergence velocity in the upper debris-covered area since 2000. We argue that this deceleration plays a key role in surface lowering, in contrast to declining surface mass balance, which we suggest is a residual effect of emergence velocity and surface lowering. Taken together, our findings indicate that the recent increase in surface lowering is attributable to the declining flux of ice from the upper to lower debris-covered areas of Lirung Glacier. Furthermore, this pattern suggests that downwasting of the upper debris-covered area will be augmented by a positive feedback between surface lowering and decelerated flow velocity.

1. Introduction

Recent changes in the volume of Himalayan glaciers not only have important implications for regional hydrology but also are spatially heterogeneous (e.g. Fujita and Nuimura, 2011; Gardelle et al., 2012a; Kääb et al., 2012). Consequently, high-resolution measurements on mass changes are required to better understand the state and fate of glaciers. However, the mass balance of debris-covered glaciers, which are the dominant glacier type in the Himalayas, is complicated by variations in supraglacial debris thickness (e.g. Nakawo and Young, 1981; Mattson et al., 1993). In situ observations have demonstrated that supraglacial material generally serves to suppress surface melting (Mattson et al., 1993; Nicholson and Benn, 2006; Zhang et al., 2011). However, recent studies utilizing remotely sensed data have suggested that debris-covered and debris-free glaciers have experienced a similar magnitude of thinning in the Himalayas (Gardelle et al., 2012a; Kääb et al., 2012; Nuimura et al., 2012). This pattern is thought to result from the formation of heat-trapping supraglacial ponds and ice cliffs, which act as hotspots and enhance ice melting beneath the debris cover (Sakai et al., 1998, 2000, 2002; Brun et al., 2016; Miles et al., 2016). In contrast, the simplified model simulations of Banerjee (2017) indicate that debris-covered glaciers exhibit similar rates of surface lowering to debris-free glaciers, due to the temporal evolution of emergence velocity profiles.

Throughout the Himalayas, regional changes in debris-covered glaciers have been evaluated using differences of remote sensing-derived digital elevation models (RS-DEMs) (Berthier et al., 2007; Bolch et al., 2011; Gardelle et al., 2012a) or a combination of multiple RS-DEMs calibrated with field surveys (Nuimura et al., 2012). For instance, a number of studies of the Khumbu region of Nepal have shown that glacier thinning has accelerated since 2000 (Bolch et al., 2011; Gardelle et al., 2012a; Nuimura et al., 2012). In central Nepal, numerous glaciological studies have evaluated the recent evolution of debris-covered glaciers in the Langtang region. For instance, in the study of Lirung Glacier, which is the focus of the present paper, Naito et al. (2002) used field data to calculate a surface-lowering rate of 1–2 m a^{-1} during the period 1996–1999 following a period of stability in the late 1980s. Over the past decade, geodetic measurements have been performed on glaciers in the Langtang region. Pellicciotti et al. (2015), for example, employed geodetic data to estimate an average mass balance of -0.32 ± 0.18 m

* Corresponding author. now at: Chiba Institute of Science, Japan.
E-mail address: tnuimura@cis.ac.jp (T. Nuimura).

http://dx.doi.org/10.1016/j.quaint.2017.06.066
1040-6182/

water equivalent (w.e.) a^{-1} for five debris-covered glaciers in the Langtang basin during the period 1974–2000. Furthermore, they reported surface-elevation changes of -0.61 ± 0.20 m a^{-1} over the debris-covered tongue of Lirung Glacier. Having extended the analysis period to 2015, Ragettli et al. (2016) reported an average geodetic mass balance for Langtang glaciers of -0.21 ± 0.08 m w.e. a^{-1} for the period 1974–2006 and -0.38 ± 0.17 m w.e. a^{-1} for 2006–2015, pointing out that considerable variability exists among individual glaciers. Focusing on the Lirung Glacier ablation zone, Ragettli et al. (2016) calculated elevation changes of -1.03 ± 0.05 m a^{-1} for the period 1974–2006 and -1.67 ± 0.59 m a^{-1} for the period 2006–2015, and also suggested that surface lowering has accelerated in recent years.

Recent refinements of survey technology have enabled high-accuracy measurements of glacier variability over relatively short time periods. For example, by deploying an Unmanned Aerial Vehicle (UAV), Immerzeel et al. (2014) created super-high resolution ortho-mosaics and DEMs of the debris-covered terminus of Lirung Glacier for May and October 2013. They then used these data to evaluate elevation changes over the lower half of the debris-covered area, which are reported as -1.09 m per 5 months (Immerzeel et al., 2014). The authors also documented intense backwasting of supraglacial ice cliffs, thereby confirming the findings of a previous study (Sakai et al., 2000, 2002), and calculated a surface velocity of 2.5 m per 5 months (Immerzeel et al., 2014). Kraaijenbrink et al. (2016) extended the analysis with additional UAV-derived aerial photography taken in May 2014, and evaluated seasonal changes in surface velocity as 6.0 m a^{-1} in summer and 2.5 m a^{-1} in winter. In this way, studies made over the past decade have revealed high-resolution changes in surface elevation and flow velocity on both long and short time scales, thanks to recent technological advances in geodetic measurements and image processing. Nonetheless, the evaluation of glacial state from the viewpoints of mass balance and ice dynamics remains poorly understood. Moreover, the remotely sensed DEMs used in geodetic measurements have room for improvement through calibration against in situ GPS surveys.

In general, variations in glacier surface elevation are a consequence of changing surface mass balance and emergence velocity, which results from differences in ice flux into and out of a specific area (Cuffey and Paterson, 2010). Conversely, average or entire surface mass balance can be estimated from difference between changes in surface elevation and in emergence velocity. This method leads to elucidate contributing factors (surface mass balance or emergence velocity) to surface elevation changes. This is also useful to evaluate representative surface mass balance of debris-covered glaciers where surface mass balance is difficult to be observed by the conventional stake method because of inaccessibility or heterogeneous surface conditions of the debris-covered area. Several previous studies have attempted this approach in the Alps (Berthier and Vincent, 2012) and the Himalaya (Nuimura et al., 2011; Vincent et al., 2016). In this study, we apply this method to a debris-covered glacier in Langtang Valley for the first time.

In the present study, we used multi-temporal DEMs (12 DEMs for the period 1974–2010) to extend the temporal coverage of surface-elevation change over the debris-covered ablation zone of Lirung Glacier in Langtang Valley, Nepal Himalaya. The advanced point of our analysis of DEMs is a calibration of remotely sensed DEMs using in situ GPS data. In addition, we explore potential factors contributing to surface lowering via a continuity equation, in which mass balance is calculated as the residual of elevation change and surface velocity, both of which are derived from satellite imagery and field surveys.

2. Study area

Lirung Glacier is located in Langtang Valley, ~60 km north of Kathmandu (Fig. 1). Below its accumulation zone on the south face of Mt. Langtang Lirung (7234 m a.s.l.), the glacier comprises a 4-km-long debris-covered ablation zone that passes beneath a steep bare rock slope (4400–4600 m elevation) (Naito et al., 2002). Similarly, glaciers throughout the Langtang Valley are typically mantled with debris below 5200 m a.s.l. (Ragettli et al., 2016). In addition, many of supraglacial ponds and ice cliffs are located the ablation zone (Sakai et al., 2000). Meteorological observations since the 1980s indicate that the majority of precipitation occurs during the summer months (e.g., 670 mm between June and September, corresponding to 55% of annual precipitation) (Seko, 1987); consequently, the region is characterized by “summer-accumulation-type” glaciation. Because accumulation and ablation both peak during the summer months, glaciers of this type are inherently more sensitive to changes in air temperature than winter-accumulation-type glaciers (Fujita and Ageta, 2000; Fujita, 2008). In Langtang Valley, multi-decadal mass-balance data for the neighboring Yala Glacier show accelerated glacier shrinkage since the 1980s (Fujita et al., 2006; Fujita and Nuimura, 2011; Sugiyama et al., 2013), the temporal pattern is supported by reanalysis of remotely sensed data (Ragettli et al., 2016).

3. Data and methods

3.1. Survey data

We used single frequency, carrier-phase differential GPS

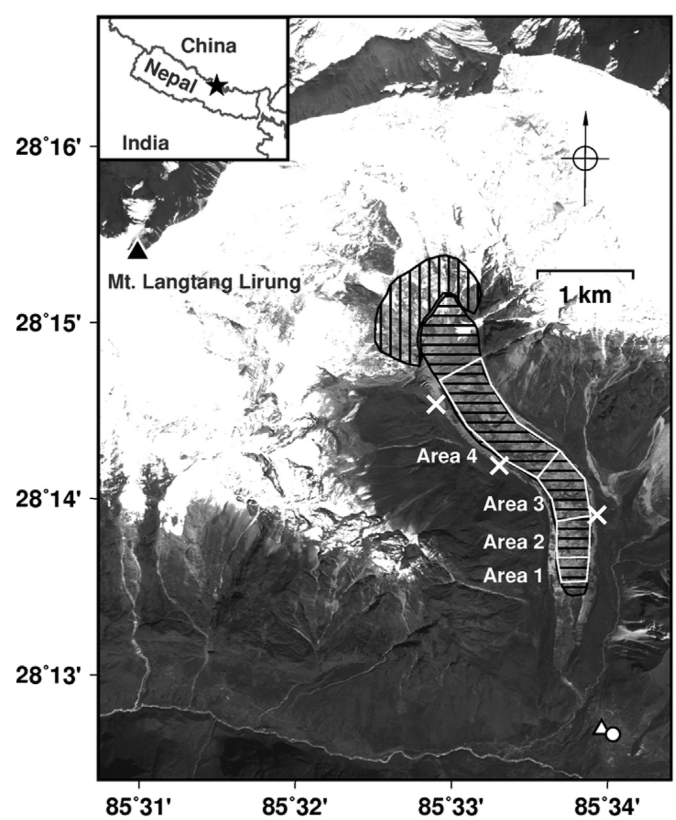

Fig. 1. Location of Lirung Glacier. The triangle, circle, white crosses, and white polygon denote a GPS base station and meteorological station at Kyangjin Village, a benchmark installed on the lateral moraine, and four areas for mass balance calculation (see Eq. (1)), respectively. The background is an ALOS PRISM image acquired on 24 October 2008.

(ProMark3, Magellan) to conduct surveys in September and October of 2008. One receiver was set at a fixed base at Kyangjin Village (3880 m a.s.l.; Fig. 1) and three additional receivers were used to survey on and around the debris-covered ablation area of Lirung Glacier. GPS data were post-processed using Global Navigation Satellite Systems Solutions software (Ashtech) and projected in the Universal Transverse Mercator projection (UTM, zone 45N, WGS-84 reference system). Measurement accuracy of a similar DGPS survey of the Bhutan Himalaya was reported as 0.11 m and 0.17 m for the horizontal and vertical axes, respectively (Fujita et al., 2008).

Measurement data for 1996 and 2008 were co-registered by referring to benchmarks located on bedrock adjacent to the glacier (Fig. 1). The benchmarks were installed in the 1980s and their relative positions surveyed using a theodolite equipped with a laser distance finder (Aoki and Asahi, 1998). Co-registered data were converted to 30-m resolution digital elevation models (DEMs), hereafter referred to as DEM_{96} and DEM_{08} for the 1996 and 2008 data respectively (Fig. 2), which in turn were used to calculate changes in glacier surface height. This conversion was carried out by regularized spline with tension, employing GRASS-GIS (Mitášová and Mitáš, 1993). Grid cells with no surveyed points were excluded so as to preclude erroneous interpolation or extrapolation. We used DEM_{08} as a reference for calibrating multi-temporal, remotely sensed DEMs (RS-DEMs).

3.2. Remotely sensed DEMs

We used five types of RS-DEM (12 DEMs in total) for the period 1974–2010 (Table 1). Although declassified KH-9 Hexagon satellite imagery is capable of producing high-resolution (6–10 m) stereo photogrammetry, the process is complicated by image distortion. To counter this effect, Surazakov and Aizen (2010) developed a method to correct for sensor distortion that utilizes IDL programming language implemented in ENVI software. We adopted their correction program for pre-processing of the Hexagon images acquired in 1974 and 1979, with which we generated two Hexagon DEMs (hereafter RS-DEM_{74} and RS-DEM_{79}, respectively). Stereo photogrammetry processing was performed using Leica Photogrammetric Suite (LPS) 2010 from ERDAS, with 3D monitor,

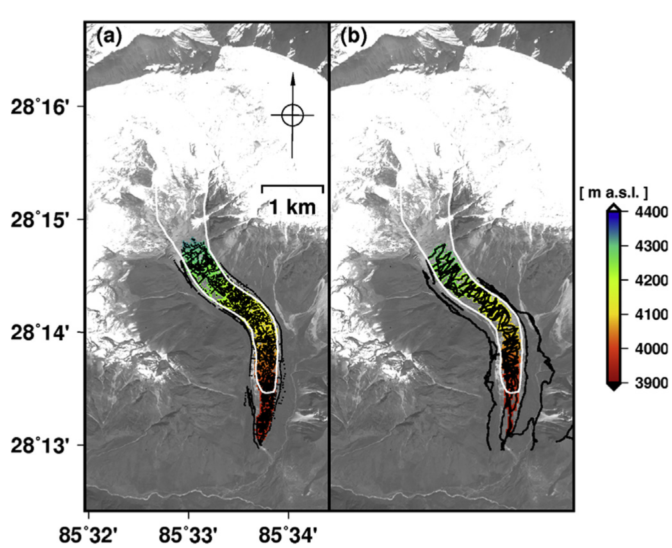

Fig. 2. Digital elevation models of the debris-covered ablation area of Lirung Glacier. DEMs were derived from field surveys in (a) 1996 and (b) 2008. Black dots indicate points measured by theodolite (a) and DGPS (b).

according to the methodology developed by Lamsal et al. (2011, 2016).

To generate a DEM for 1992 (hereafter RS-DEM_{92}), we employed a 1: 50,000 scale topographic map based on aerial photography from that year, which was originally published by the Survey Department of Nepal. We converted the digitized 40 m-contour-interval data to a 30-m-resolution DEM using a regularized spline with tension (Mitášová and Mitáš, 1993). The reported horizontal accuracy of the map-derived DEM is ~18 m (Salerno et al., 2008).

We used the Shuttle Radar Topographic Mission (SRTM) DEM, corrected in February 2000 (https://dds.cr.usgs.gov/srtm/version2_1/; last accessed on 19 October 2016), as our data set for that year (hereafter RS-DEM_{00}). Specifically, we resampled the original SRTM3 data (3 arcsec, ~90 m) at 30 m resolution (UTM, zone 45N, WGS-84 reference system) using bilinear interpolation implemented in the GeoSpatial Data Abstraction Library (GDAL). Two previous studies used this DEM to determine ice surface elevations in 1999 due to penetration of the SRTM C-band radar into surface snow (Gardelle et al., 2012b; Kääb et al., 2012). In our study, we considered the DEM as the surface height in 2000 because of our targeted debris-covered surface.

To create DEMs for 2001, 2003, and 2004 (hereafter RS-DEM_{01}, RS-DEM_{03}, and RS-DEM_{04}, respectively), we selected cloud-free scenes from Advanced Spaceborne Thermal Emission Reflection Radiometer (ASTER) imagery, provided by the Japanese Earth Remote Sensing Data Analysis Center (ERSDAC). Further details on the generation of these DEMs are given by Fujisada et al. (2005) and Toutin (2008), in addition to the ASTER science project website (http://www.aster.jspacesystems.or.jp/en/; last accessed on 13 October 2016). For our most recent DEMs, we used the Advanced Land Observing Satellite Panchromatic Remote-sensing Instrument for Stereo Mapping (ALOS-PRISM), provided by the Japan Aerospace Exploration Agency (JAXA). Specifically, we created two separate DEMs for 2008 (RS-DEM_{08a} and RS-DEM_{08b}) from ALOS-PRISM imagery taken in January and October of that year, respectively, in conjunction with DSM and Ortho-image Generation Software developed by JAXA for ALOS PRISM (DOCS-AP). We used the same method to create a DEM for 2010 (RS-DEM_{10}) from the Hexagon KH-9-derived DEM with LPS with 3D monitor.

3.3. Bias calibration

Remotely sensed DEMs commonly include errors related to data acquisition, such that a bias calibration is required prior to DEM differencing. We used a co-registration process to improve elevation residuals among our DEMs. Specifically, we co-registered each RS-DEM against DEM_{08} by minimizing the standard deviation of elevation difference over the off-glacier terrain, where zero elevation change is expected (Nuimura et al., 2012). In addition, we adjusted vertically the elevation of co-registered RS-DEMs by subtracting the respective mean elevation differences from DEM_{08}. Table 1 gives the standard deviations of elevation difference after each co-registration and vertical adjustment.

For DEMs derived from Hexagon KH-9 (RS-DEM_{74} and RS-DEM_{79}), we observed a north–south bias trend that potentially results from insufficient adjustment of triangulation parameters. We calculated this bias trend by referring to the gap-filled SRTM version 4 (Rabus et al., 2003). First, we calculated differences between the two DEMs over gently sloping (<10°) off-glacier terrain. Second, having excluded outliers (elevation difference >100 m), we approximated the regression of 2nd order multi-variables (northing and easting). We also excluded outliers that exceeded the standard deviation between the original elevation and the estimated elevation on approximated regression planes. Finally, we calibrated the Hexagon KH-9-derived DEMs by subtracting the

Table 1
Remote sensing data list.

	Year	Note	Original σ [m]	Adjusted σ[m]
Hexagon	Nov. 1974	Photogrammetry by LPS 3D	9.2	8.9
Hexagon	Apr. 1979	Photogrammetry by LPS 3D	18.0	14.8
Map	1992	Contour (40 m Int.)	15.7	12.3
SRTM	Feb. 2000	SRTM3 v.2.1 by USGS	14.6	11.0
ASTER	Oct. 2001	L3A01 product by ERSDAC	13.4	13.4
ASTER	Oct. 2003	L3A01 product by ERSDAC	12.2	12.2
ASTER	Oct. 2004	L3A01 product by ERSDAC	14.5	14.2
ALOS	Jan. 2008	Photogrammetry by LPS 3D	5.1	4.8
ALOS	Oct. 2008	Photogrammetry by LPS 3D	7.9	7.5
ALOS	Jan. 2009	Photogrammetry by LPS 3D	5.6	5.3
ALOS	Jan. 2009	Photogrammetry by LPS 3D	8.0	7.7
ALOS	Dec. 2010	Photogrammetry by LPS 3D	10.1	10.0

elevation difference between the regression plane and the reference DEM (SRTM version 4).

3.4. Delineation of glacier area

The accumulation and ablation zones of Lirung Glacier are separated by a steep rock slope between 4400 and 4600 m a.s.l. The ablation zone, which is the focus of this study, lies entirely below 4400 m elevation and is delineated using ASTER false-color imagery from 2004. On the basis of our field observations, we excluded the lowermost part of the ablation zone from our investigation since no surface change was detected during the study period.

3.5. Elevation change

DEM differencing was calculated from DEM_{96} and DEM_{08} and is defined here as Δh_{96-98}. Prior to the rasterization of point survey data, we excluded any data points from off-glacier terrain (e.g., lateral moraines). We also used glacier surface elevation change to delineate the debris-covered glacier terminus. Differences of remotely sensed DEMs is directly affected by errors in each RS-DEM. Therefore, to minimize the impact of this error, differencing is typically performed using as long a period of DEM coverage as possible (Bolch et al., 2011). The analytical correction of systematic DEM bias is also an effective means to reducing error (Nuth and Kääb, 2011; Gardelle et al., 2012a). In this study, we calculated elevation change as a linear regression with weighted least squares (WLS) for each grid cell (Nuimura et al., 2012), using multi-temporal RS-DEMs during four periods: 1974–2000, 1974–2010, 2000–2008, and 2000–2010 (hereafter Δh_{74-00}, Δh_{74-10}, Δh_{00-08} and Δh_{00-10}, respectively). The weight used to calculate linear regression with WLS is the accuracy of each RS-DEM (adjusted σ in Table 1). Finally, calculated values of Δh_{00-08} were compared to the findings of our field survey (Δh_{96-08}).

3.6. Flow velocity

Ice-stake measurements show that surface flow velocities on Lirung Glacier were 5.7–6.0 m a^{-1} in the upper debris-covered area between September 1994 and October 1996, and 0.8–2.1 m a^{-1} in the lower debris-covered area between December 1989 and October 1996 (Naito et al., 1998). More recently, surface flow velocity was calculated as subpixel displacements using a phase correlation algorithm implemented in the COSI-Corr plug-in module for ENVI (Leprince et al., 2007). In our assessment, we used 2.5-m-resolution ortho-rectified ALOS PRISM imagery, taken in October 2008 and December 2010. First, we determined the scene-wide subpixel bias by calculating displacement over the off-glacier area, where no displacement is expected, in both easterly and northerly directions. After excluding >100 grid displacements as extreme outliers, we then calculated the median displacement as 3.0 m and removed any cells that differed from the median by more than six standard deviations. We repeated the process with the remaining grids using a median of 0.0 m and excluding those that fell more than three standard deviations beyond the median. Calculated values for displacement of the glacier surface were screened using magnitude and direction filters according to Scherler et al. (2008). We then rejected any absolute displacement grid that differed from the scalar median within a moving window by more than one standard deviation. In addition, we excluded any grid that deviated by > 60° from the median direction, which is calculated within a moving window of 51 × 51 grid size (corresponding to 127.5 m on the ground) by visual trial and error.

Uncertainty in surface displacement results mainly from image contrast. For example, uncertainties in snow-covered high-altitude areas differ from those in snow-free low-altitude areas. To evaluate the uncertainty in surface displacement over the debris-covered area, we calculated the altitudinal distribution of mean displacement using the digital number of satellite imagery (0–255) for the off-glacier area (Fig. 3). Fig. 3 demonstrates that large displacements occur in snow-covered (high digital number) higher-altitude (>4400 m a.s.l.) areas, and vice versa. At higher elevations, the mean displacement of on- and off-glacier grids is 7.8 and 7.4 m a^{-1}, respectively, while at low (<4400 m a.s.l.) elevations the equivalent values are 2.7 and 0.8 m a^{-1}, respectively. Therefore, we assume that displacement uncertainty on the debris-covered area is 0.8 m a^{-1}.

3.7. Deriving mass balance from elevation change and emergence velocity

To evaluate factors controlling the observed changes in ice surface elevation, we calculated mass balance for the four domains in the debris-covered area of Lirung Glacier (Fig. 1) using a continuity equation (Cuffey and Paterson, 2010), in which values for elevation change and emergence velocity are required. A change in glacier thickness within a certain part of a glacier is defined as

$$\frac{\delta H}{\delta t} = b + \frac{(Q_{in} - Q_{out})}{\overline{W} \cdot \delta x} \tag{1}$$

where Q is the ice flux entering (in) and leaving (out) the area of interest, H is ice thickness, t is a given time, b is surface mass balance (which is equivalent to ablation of debris-covered ice), $\overline{W}$ is the averaged glacier width, and x is the longitudinal length of the area of interest. The second term on the right in Eq. (1) describes the emergence velocity resulting from glacier flow convergence (Cuffey and Paterson, 2010). Ice flux at a boundary of the area of interest is described as

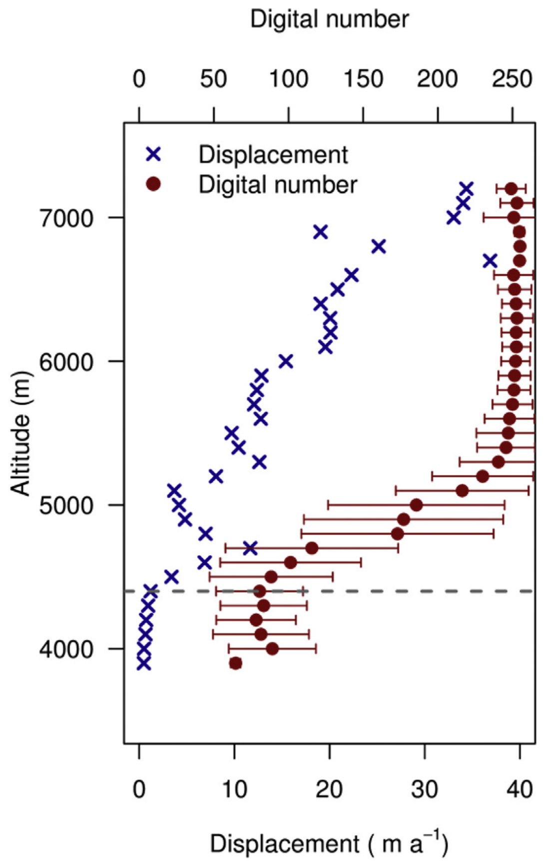

Fig. 3. Altitudinal distribution of displacement biases and digital numbers of an ALOS PRISM image (24 October 2008), which is given as an index of surface contrast.

$$Q = WHv \tag{2}$$

where v is the flow velocity at the upper or lower edge of the box for the continuity equation. The depth averaged velocity was set as 80% of the mean surface velocity according to the manner of Sakai et al. (2006) and Cuffey and Paterson (2010). Because the surface velocity data for the older period (1974–2000) do not correspond to boundary of the four domains strictly, the flow velocity at the boundaries are linearly interpolated and extrapolated from the survey data by Naito et al. (1998). We obtained values for glacier width from satellite imagery. We used glacier thickness, which was determined originally via radio-echo sounding in 1999 (Gades et al., 2000), against surface-elevation changes for each period. We then applied both surveyed (Naito et al., 1998) and calculated (this study) values for surface-flow velocity. Each parameter is listed in Table 2.

4. Results

4.1. Validation of remote sensing data with field observations

Elevation changes were calculated by DEM differencing for the period 1996–2008, based on field measurements (Fig. 4a), and by linear regression with WLS for the period 2000–2008, from multi-temporal RS-DEMs (Fig. 4b). Because access to the uppermost debris-covered ice surface is limited, the area for Δh_{96-08} is smaller than that for Δh_{00-08}. By comparing common grids in two products (<4400 m a.s.l.; n = 895), the elevation changes between these two measurement periods are -1.13 ± 0.82 m a^{-1} for Δh_{96-08} and -1.62 ± 1.04 m a^{-1} for Δh_{00-08}.

Extensive areas of glacier downwasting are evident in both periods, but are particularly prominent (>3 m a^{-1} surface lowering) in the uppermost debris-covered area for Δh_{00-08}, for which in situ survey data are unavailable. Although the two periods are not identical, the magnitude of elevation change between the two exhibits a weakly significant correlation ($r = 0.51$, $p < 0.01$). This similarity indicates that estimates of elevation change derived from remote sensing are reliable and comparable to field-based estimates. Similarly, the spatial distribution of uncertainties in elevation change derived from multi-temporal RS-DEMs are small over the debris-covered area, although larger uncertainties (>1 m a^{-1}) occur over the high-altitude accumulation zone (Fig. 4c). Large uncertainties have also been observed over the accumulation zones of glaciers in the Khumbu region using the same method (Nuimura et al., 2012). However, this pattern does not affect the current study, which focuses on elevation changes in the debris-covered area.

4.2. Surface elevation change

Estimates of elevation change from multi-temporal RS-DEMs were calculated for the periods 1974–2010 (Δh_{74-10}), 1974–2000 (Δh_{74-00}), and 2000–2010 (Δh_{00-10}) using linear regression with WLS. Values for the debris-covered area of Lirung Glacier are -1.07 ± 0.42 m a^{-1} for Δh_{74-10}, -0.78 ± 0.43 m a^{-1} for Δh_{74-00}, and -1.99 ± 1.41 m a^{-1} for Δh_{00-10}, and together indicate a pattern of overall downwasting (Fig. 5). Significant downwasting of the upper debris-covered area is evident for both the longest and most recent periods (Δh_{74-10} and Δh_{00-10}, respectively; Fig. 5a and c), yet is absent from the period 1974–2000 (Δh_{74-00}; Fig. 5b). In addition, considerable downwasting also occurred in the lowermost debris-covered area with clear margin at the lower bound suggesting the glacier terminus. A comparison of elevation-change values prior to and after 2000 (Δh_{74-00} and Δh_{00-10}) indicates accelerated downwasting since 2000, a pattern also supported by longitudinal profiles of elevation change (Fig. 6a). We estimate that the modern debris-covered glacier terminus is located ~800 m up-valley from its analyzed area of the Δh_{96-08} period. The magnitude of downwasting indicated by Δh_{00-10}(1.99 m a^{-1}) is comparable to or higher than that of glaciers affected by growth of with expanding large supraglacial lakes at the terminus in the Khumbu region, which is located in a similar climatic and geographic setting to that of the present study (Bolch et al., 2011; Nuimura et al., 2012). For instance, estimates of thinning for the debris-covered Imja Glacier range from -1.45 m a^{-1} (Bolch et al., 2011) to -0.93 m a^{-1} (Nuimura et al., 2012) for the period 2002–2007.

4.3. Surface flow velocity

The distribution of flow velocity data suggests a gradual velocity increase in the upper-to-middle parts of the debris-covered area and a gradual decrease in the lower part (Figs. 6b and 7). In the upper part, adjacent to the bedrock slope separating the ablation and accumulation zones, we observed no apparent displacement (Fig. 7). Similarly, the vector field in this area indicates surface movement from high-angle northern and western slopes onto the glacier surface, a pattern that is suggestive of accumulation through snow avalanching rather than displacement by glacier flow. Compared with data from the 1980s and 1990s (Naito et al., 1998), our data exhibit a significant decrease in flow velocity (from 6 to 2–3 m a^{-1}) within the upper part of the debris-covered area but similar velocities (1–2 m a^{-1}) in the lower ablation area (Fig. 6b).

4.4. Continuity equation

To estimate uncertainty of mass balance and emergence

Table 2
Temporal changes in elevation, emergence and mass balance in each areas for the periods 1974–2000 and 2000–2010.

Area	Year	Elevation change (m a^{-1})	Emergence velocity (m a^{-1})	Mass balance (m a^{-1})
1	1974–2000	−1.27 ± 0.16	0.10 ± 0.03	−1.37 ± 0.18
2	1974–2000	−1.18 ± 0.16	0.26 ± 0.06	−1.44 ± 0.22
3	1974–2000	−1.14 ± 0.17	0.22 ± 0.07	−1.36 ± 0.24
4	1974–2000	−0.63 ± 0.18	0.35 ± 0.06	−0.98 ± 0.24
1	2000–2010	−1.82 ± 0.27	0.08 ± 0.07	−1.90 ± 0.33
2	2000–2010	−1.59 ± 0.19	0.17 ± 0.10	−1.75 ± 0.30
3	2000–2010	−1.30 ± 0.25	0.19 ± 0.11	−1.49 ± 0.35
4	2000–2010	−1.69 ± 0.25	0.00 ± 0.07	−1.69 ± 0.32

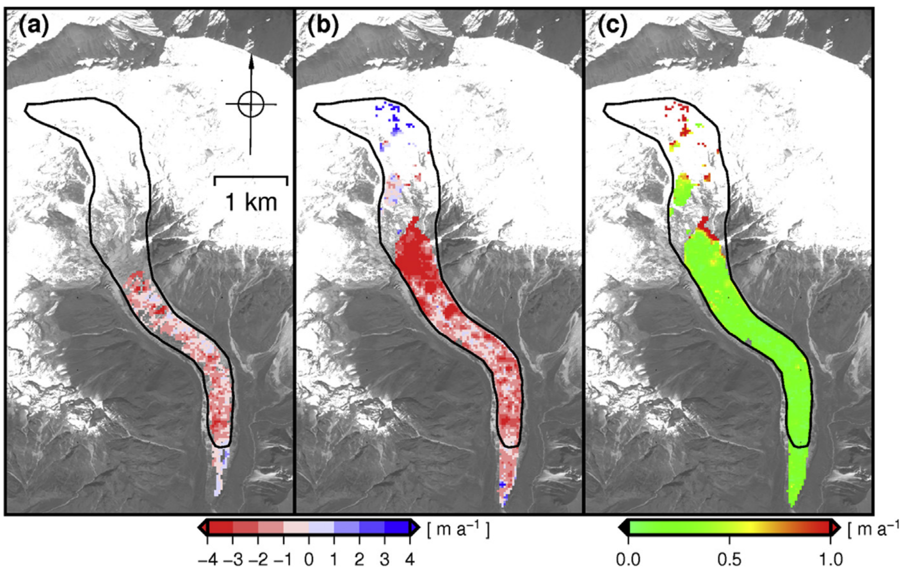

Fig. 4. Distribution of elevation changes over the Lirung Glacier ablation zone for the periods (a) 1996–2008 and (b) 2000–2008. (c) Estimated error for the period 2000–2008.

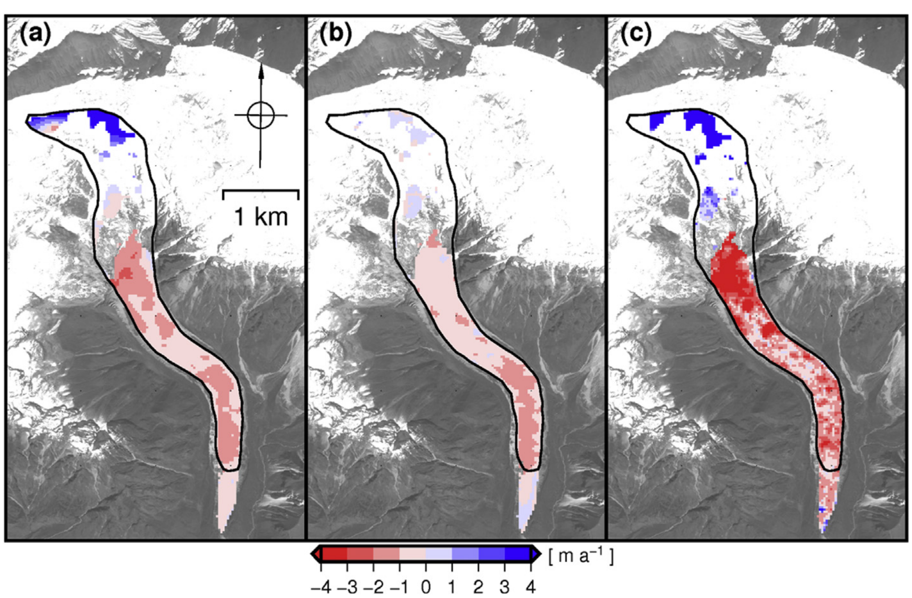

Fig. 5. Distribution of elevation changes over the Lirung Glacier ablation zone for the periods (a) 1974–2010, (b) 1974–2000, and (c) 2000–2010.

velocity, we evaluated error propagation from original errors. Original errors of the surface elevation change in four domains are calculated as average of error from linear regression with WLS. We assume reading errors of width (w) and length (x) of the glacier to be 5 m, which correspond to two cell size of ALOS PRISM. The glacier thickness errors are reported as 5 m around terminus and 10 m around upper debris-covered part (Gades et al., 2000). Therefore, we assume the thickness error of 5 m for Area 1, and that

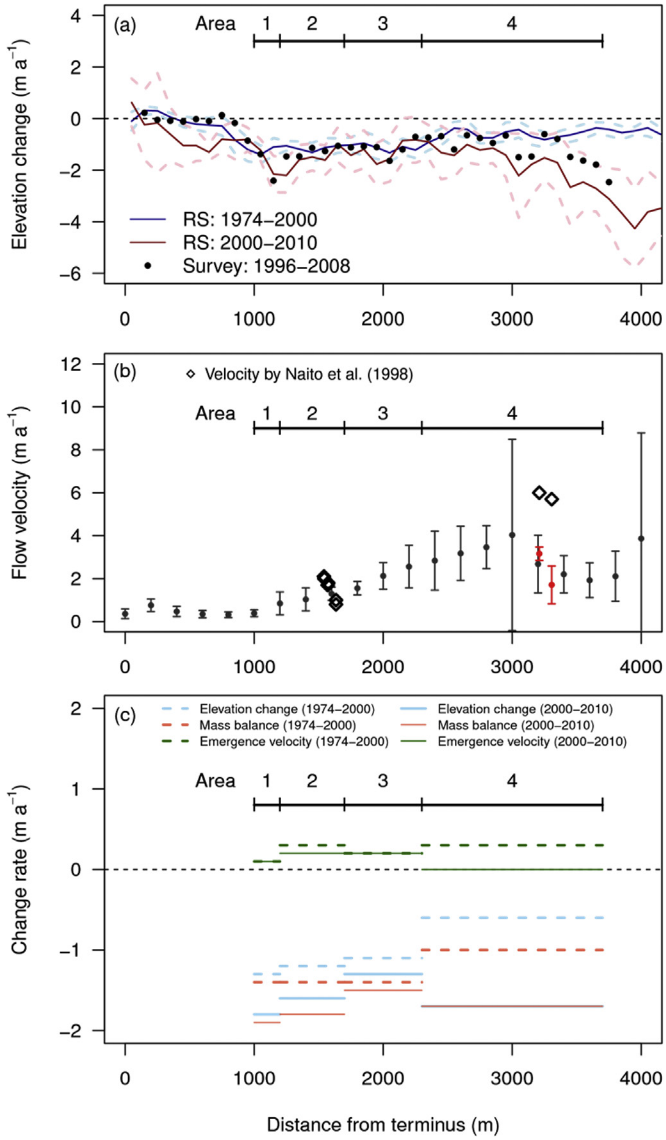

Fig. 6. Longitudinal profiles of (a) elevation change for the periods 1974–2000, 2000–2010, and 1996–2008; (b) in situ surveyed and remotely sensed flow velocities; and (c) components in the continuity equation for the four areas of the debris-covered area of Lirung Glacier (see Fig. 1). Black circles with error bars in (b) denote the average value and the standard deviation of the velocity for distance bins of 200 m, respectively. Red circles with error bars in (b) denote the average value and the standard deviation of the velocity for 50 m buffer distance from survey points in upper debris-covered area by Naito et al. (1998). (For interpretation of the references to colour in this figure legend, the reader is referred to the web version of this article.)

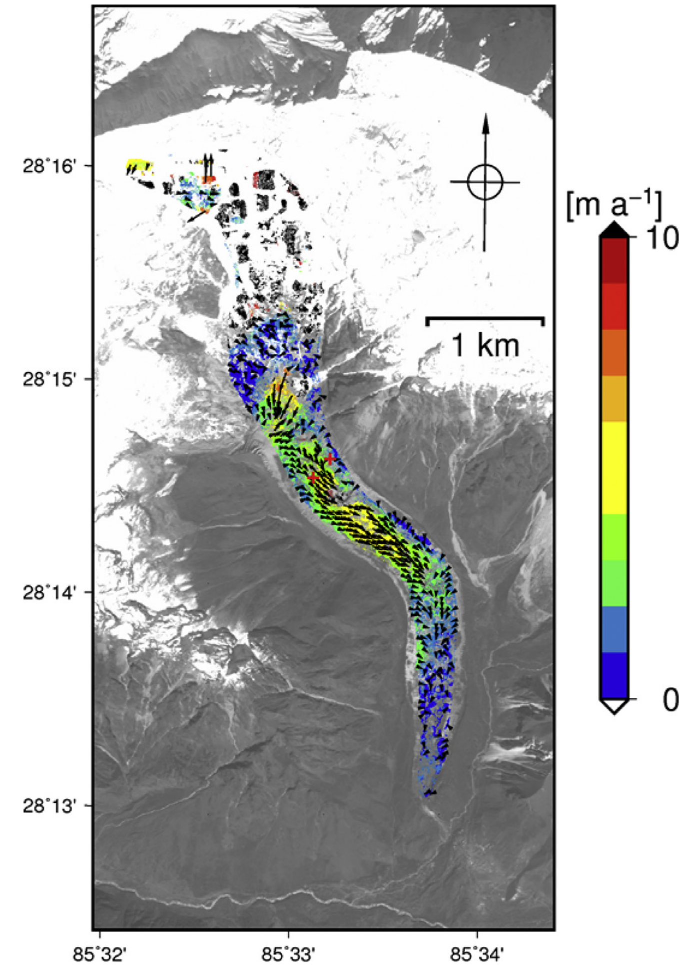

Fig. 7. Distribution of displacement portrayed as flow velocity over the Lirung Glacier ablation zone. Vectors indicate flow direction. Two red cross show survey points in upper debris-covered area by Naito et al. (1998). (For interpretation of the references to colour in this figure legend, the reader is referred to the web version of this article.)

of 10 m for Areas 2–4 conservatively. Displacement error by stake measurement is assumed to be 0.02 m by referring ±0.01 m for single measurement (Vincent et al., 2016). Another displacement error by remote sensing analysis is assumed to be 0.63 m by referring 25% of pixel size (Heid and Kääb, 2012).

Surface lowering occurred throughout the debris-covered area and has accelerated since 2000. Whereas Areas 1–3 exhibit no significant change in emergence velocity for both periods (1974–2000 and 2000–2010) (Fig. 6c, Table 2), Area 4 underwent a significant decrease in emergence velocity (from 0.35 ± 0.06 m a^{-1} to 0.00 ± 0.04 m a^{-1}). Mass balance, calculated as the residual of elevation change and emergence velocity (Eq. (1)), was generally negative throughout the debris-covered area (from −1.37 ± 0.18 m a^{-1} to −1.90 ± 0.33 m a^{-1} in Area 1; from −1.44 ± 0.22 m a^{-1} to −1.75 ± 0.30 m a^{-1} in Area 2; from −1.36 ± 0.24 m a^{-1} to −1.49 ± 0.35 m a^{-1} in Area 3; from −0.98 ± 0.24 m a^{-1} to −1.69 ± 0.32 m a^{-1} in Area 4). The decrease in mass balance corresponds to increased ablation, which in turn results from declining emergence velocities.

Accelerated surface lowering of the debris-covered area since 2000 is likely due to increased ablation, and in the upper ablation area this has been reinforced by declining emergence velocity. The longitudinal profile of flow velocity supports this interpretation (Fig. 6c, Table 2), which has also been observed at Khumbu Glacier (Nuimura et al., 2011). The reduced flux of ice into the ablation zone potentially reflects declining accumulation at higher altitudes, which is evident in regional ice-core records (Fujita et al., 2006).

5. Discussion

5.1. Accelerated surface lowering

Multi-temporal analysis of remotely sensed DEMs reveals that the debris-covered surface of Lirung Glacier has been lowering since at least 1974 and that this process accelerated after 2000. The measured change in elevation for Δh_{74-00}(−0.78 ± 0.43 m a^{-1}) is similar to that derived by Pellicciotti et al. (2015) for the period 1974–1999 (−0.61 ± 0.11 m a^{-1}) based on differencing of a similar set of RS-DEMs.

Similarly, the recent acceleration in surface lowering from −0.78 m a^{-1} (1974–2000) to −1.99 m a^{-1} (2000–2010) is consistent with the findings of Ragettli et al. (2016), who estimated that the rate of thinning increased from −1.03 ± 0.05 m a^{-1} (1974–2006) to −1.67 ± 0.59 m a^{-1} (2006–2015).

For the period 1974–2000, the most significant surface lowering occurred on the lower part of the ablation zone, with less extreme rates in the middle part; in contrast, the greatest rates of thinning during the period 2000–2010 occurred in the upper ablation zone (Figs. 5c and 6a). The progressive down-glacier expansion of intensified downwasting over the past decade is consistent with the flow velocity profile, which depicts flow velocities in the middle–upper areas decreasing during the 1990s (Fig. 6b) whereas the flow velocity significantly decreased around 3–4 km from terminus (Fig. 6b). Intensified surface lowering of the upper ablation zone in the past decade is further supported by the findings of Ragettli et al. (2016), who reconstructed changes in the longitudinal surface profile for the periods 1974–2009 and 2006–2015. Both profiles show the development of enhanced thinning zones around 4300 m a.s.l., which corresponds to the upper part of the debris-covered area of Lirung Glacier. The increase of flow velocity from the upper part toward down-glacier (around 3500–3000 m from the terminus) results in decreased emergence velocities, which in turn enhances surface lowering in the same area (Fig. 6c). This pattern suggests that accelerated surface lowering of the debris-covered area since 2000 is due largely to decreased flow velocity.

As we described in section 4.2, glaciers with large terminal glacial lakes have high rate of lowering in the Khumbu region (Imja and Lumding) (Bolch et al., 2011; Nuimura et al., 2012). The formation of a terminal lake would reduce compression in the lowermost part of the glacier. Therefore, the rapid surface lowering of those glaciers supporting supraglacial lakes can be attributed to decreased emergence velocity at the terminus. In contrast, we propose that the rapid surface lowering of the upper debris-covered Lirung Glacier is a consequence of declining emergence velocity due to reduced accumulation.

5.2. Fate of the debris-covered area

Past measurements have shown that the debris-covered area of Lirung Glacier was between 90 and 120 m thick in its middle and upper reaches (Gades et al., 2000). Assuming a constant rate of elevation change of −1.07 ± 0.11 m a^{-1} (Δh_{74-00}), the debris-covered glacier tongue will likely persist for a further 84–112 years, or for 45–60 years according to the higher rate of −1.99 ± 1.41 m a^{-1} (Δh_{00-10}). Alternatively, if the maximum thinning rate observed in the upper ablation zone during the last decade (−4 m a^{-1}; Δh_{00-10}, Fig. 6a) is maintained, the ice in that area will likely disappear within 23–30 years. Glacier thinning and deceleration serve as mutually positive feedback mechanisms. Two potential factors might account for the decrease in emergence velocity in the upper area (Area 4) are (1) decreased mass input due to declining accumulation in the accumulation zone and (2) a weakened flow-velocity gradient due to extreme glacier thinning in the uppermost debris-covered area (above Area 4).

6. Conclusions

We used field surveys and multi-temporal remote sensing to evaluate surface-elevation changes over the debris-covered ablation zone of Lirung Glacier. Taken together, the data suggest that estimates derived from RS-DEMs are consistent with those obtained from in situ surveyed DEMs, which show that surface lowering has continued since at least 1974 over the entire debris-covered area. Surface lowering accelerated after 2000 and has been greatest in the uppermost reaches of the ablation zone, where ice flow velocity decreased significantly between the 1990s and 2010. Using the continuity equation, we evaluated the relative contributions of changing surface mass balance and emergence velocity to the observed surface lowering. This approach demonstrates that the increasingly negative mass balance across the debris-covered area has played a significant role in surface lowering. In addition, declining flow velocity in the upper part of the ablation zone has weakened emergence velocity, further enhancing the pattern of surface lowering.

Acknowledgements

We thank the Department of Hydrology and Meteorology of the Ministry of Science and Technology, Nepalese Government, and Guide for All Seasons Trek for field support and logistics. We also thank the USGS for making available Hexagon and SRTM3 DEM version 2.1, and JAXA for use of the ALOS-PRISM derived DEM. We are grateful to F. Salerno and an anonymous reviewer for their thoughtful comments. Field observations and analyses were supported by JSPS-KAKENHI grant numbers 19253001 and 26257202, as well as a grant from the Funding Program for Next Generation World-Leading Researchers (NEXT Program, GR052).

References

Aoki, T., Asahi, K., 1998. Topographical map of the ablation area of the lining glacier in the Langtang Valley, Nepal Himalaya. Bull. Glacier Res. 16, 19–31.

Banerjee, A., 2017. Brief communication: thinning of debris-covered and debris-free glaciers in a warming climate. Cryosphere 11, 133–138. http://dx.doi.org/10.5194/tc-11-133-2017.

Berthier, E., Arnaud, Y., Kumar, R., Ahmad, S., Wagnon, P., Chevallier, P., 2007. Remote sensing estimates of glacier mass balances in the Himachal Pradesh (Western Himalaya, India). Remote Sens. Environ. 108, 327–338. http://dx.doi.org/10.1016/j.rse.2006.11.017.

Berthier, E., Vincent, C., 2012. Relative contribution of surface mass-balance and ice-flux changes to the accelerated thinning of Mer de Glace, French Alps, over 1979–2008. J. Glaciol. 58, 501–512. http://dx.doi.org/10.3189/2012JoG11J083.

Bolch, T., Pieczonka, T., Benn, D., 2011. Multi-decadal mass loss of glaciers in the Everest area (Nepal Himalaya) derived from stereo imagery. Cryosphere 5, 349–358. http://dx.doi.org/10.5194/tc-5-349-2011.

Brun, F., Buri, P., Miles, E.S., Wagnon, P., Steiner, J., Berthier, E., Ragettli, S., Kraaijenbrink, P., Immerzeel, W.W., Pellicciotti, F., 2016. Quantifying volume loss from ice cliffs on debris-covered glaciers using high-resolution terrestrial and aerial photogrammetry. J. Glaciol. 62, 684–695. http://dx.doi.org/10.1017/jog.2016.54.

Cuffey, K.M., Paterson, W.S.B., 2010. The Physics of Glaciers, fourth ed. Butterworth-Heinemann, Oxford.

Fujisada, H., Bailey, G., Kelly, G., Hara, S., Abrams, M., 2005. ASTER DEM performance. IEEE Trans. Geosci. Remote Sens. 43, 2707–2714. http://dx.doi.org/10.1109/TGRS.2005.847924.

Fujita, K., 2008. Effect of precipitation seasonality on climatic sensitivity of glacier mass balance. Earth Planet. Sci. Lett. 276, 14–19. http://dx.doi.org/10.1016/j.epsl.2008.08.028.

Fujita, K., Ageta, Y., 2000. Effect of summer accumulation on glacier mass balance on the Tibetan Plateau revealed by mass-balance model. J. Glaciol. 46, 244–252. http://dx.doi.org/10.3189/172756500781832945.

Fujita, K., Nuimura, T., 2011. Spatially heterogeneous wastage of Himalayan glaciers. Proc. Natl. Acad. Sci. U. S. A. 108 http://dx.doi.org/10.1073/pnas.1106242108, 14 011–14 014.

Fujita, K., Thompson, L., Ageta, Y., Yasunari, T., Kajikawa, Y., Sakai, A., Takeuchi, N., 2006. Thirty-year history of glacier melting in the Nepal Himalayas. J. Geophys. Res. 111, 3–8. http://dx.doi.org/10.1029/2005JD005894.

Fujita, K., Suzuki, R., Nuimura, T., Sakai, A., 2008. Performance of ASTER and SRTM DEMs, and their potential for assessing glacial lakes in the Lunana region, Bhutan Himalaya. J. Glaciol. 54, 220–228. http://dx.doi.org/10.3189/002214308784886162.

Gades, A., Conway, H., Nereson, N., Naito, N., Kadota, T., 2000. Radio echo-sounding through supraglacial debris on Lirung and Khumbu glaciers, Nepal Himalayas. IAHS Publ. 264, 13–22.

Gardelle, J., Berthier, E., Arnaud, Y., 2012a. Slight mass gain of Karakoram glaciers in the early twenty-first century. Nat. Geosci. 5, 1–4. http://dx.doi.org/10.1038/ngeo1450.

Gardelle, J., Berthier, E., Arnaud, Y., 2012b. Impact of resolution and radar penetration on glacier elevation changes computed from DEM differencing. J. Glaciol. 58, 419–422. http://dx.doi.org/10.3189/2012JoG11J175.

Heid, T., Kääb, A., 2012. Evaluation of existing image matching methods for deriving

glacier surface displacements globally from optical satellite imagery. Remote Sens. Environ. 118, 339–355. http://dx.doi.org/10.1016/j.rse.2011.11.024.
Immerzeel, W.W., Kraaijenbrink, P.D.A., Shea, J.M., Shrestha, A.B., Pellicciotti, F., Bierkens, M.F.P., de Jong, S.M., 2014. High-resolution monitoring of Himalayan glacier dynamics using unmanned aerial vehicles. Remote Sens. Environ. 150, 93–103. http://dx.doi.org/10.1016/j.rse.2014.04.025.
Kääb, A., Berthier, E., Nuth, C., Gardelle, J., Arnaud, Y., 2012. Contrasting patterns of early twenty-first-century glacier mass change in the Himalayas. Nature 488, 495–498. http://dx.doi.org/10.1038/nature11324.
Kraaijenbrink, P., Meijer, S.W., Shea, J.M., Pellicciotti, F., De Jong, S.M., Immerzeel, W.W., 2016. Seasonal surface velocities of a Himalayan glacier derived by automated correlation of unmanned aerial vehicle imagery. Ann. Glaciol. 57 (71), 103–113. http://dx.doi.org/10.3189/2016AoG71A072.
Lamsal, D., Sawagaki, T., Watanabe, T., 2011. Digital terrain modelling using Corona and ALOS PRISM data to investigate the distal part of Imja Glacier, Khumbu Himal, Nepal. J. Mt. Sci. 8, 390–402. http://dx.doi.org/10.1007/s11629-011-2064-0.
Lamsal, D., Fujita, K., Sakai, A., 2016. Moderate mass loss of Kanchenjunga Glacier in the eastern Nepal Himalaya since 1975 revealed by Hexagon KH-9 and ALOS satellite imageries. Cryosphere Discuss. http://dx.doi.org/10.5194/tc-2016-202 in review.
Leprince, S., Barbot, S., Ayoub, F., Avouac, J., 2007. Automatic and precise orthorectification, coregistration, and subpixel correlation of satellite images, application to ground deformation measurements. IEEE Trans. Geosci. Remote Sens. 45, 1529–1558. http://dx.doi.org/10.1109/TGRS.2006.888937.
Mattson, L., Gardner, J., Young, G., 1993. Ablation on debris covered glaciers: an example from the Rakhiot Glacier, Punjab, Himalaya. IAHS Publ. 218, 289–296.
Miles, E.S., Pellicciotti, F., Willis, I.C., Steiner, J.F., Buri, P., Arnold, N.S., 2016. Refined energy-balance modelling of a supraglacial pond, Langtang Khola, Nepal. Ann. Glaciol. 57 (71), 29–40. http://dx.doi.org/10.3189/2016AoG71A421.
Mitášová, H., Mitáš, L., 1993. Interpolation by regularized spline with tension: I. Theory and implementation. Math. Geol. 25, 641–655. http://dx.doi.org/10.1007/BF00893171.
Naito, N., Nakawo, M., Aoki, T., Asahi, K., Fujita, K., Sakai, A., Kadota, T., Shiraiwa, T., Seko, K., 1998. Surface flow on the ablation area of the Lirung Glacier in Langtang Valley, Nepal Himalayas. Bull. Glacier Res. 16, 67–73.
Naito, N., Kadota, T., Fujita, K., Sakai, A., Nakawo, M., 2002. Surface lowering over the ablation area of Lirung Glacier, Nepal Himalayas. Bull. Glaciol. Res. 19, 41–46.
Nakawo, M., Young, G., 1981. Field experiments to determine the effect of a debris layer on ablation of glacier ice. Ann. Glaciol. 2, 85–91. http://dx.doi.org/10.3189/172756481794352432.
Nicholson, L., Benn, D.I., 2006. Calculating ice melt beneath a debris layer using meteorological data. J. Glaciol. 52, 463–470. http://dx.doi.org/10.3189/172756506781828584.
Nuimura, T., Fujita, K., Fukui, K., Asahi, K., Aryal, R., Ageta, Y., 2011. Temporal changes in elevation of the debris-covered ablation area of Khumbu Glacier in the Nepal Himalaya since 1978. Arct. Antarct. Alp. Res. 43, 246–255. http://dx.doi.org/10.1657/1938-4246-43.2.246.
Nuimura, T., Fujita, K., Yamaguchi, S., Sharma, R., 2012. Elevation changes of glaciers revealed by multitemporal digital elevation models calibrated by GPS survey in the Khumbu region, Nepal Himalaya, 1992–2008. J. Glaciol. 58, 648–656. http://dx.doi.org/10.3189/2012JoG11J061.
Nuth, C., Kääb, A., 2011. Co-registration and bias corrections of satellite elevation data sets for quantifying glacier thickness change. Cryosphere 5, 271–290. http://dx.doi.org/10.5194/tc-5-271-2011.
Pellicciotti, F., Stephan, C., Miles, E., Herreid, S., Immerzeel, W.W., Bolch, T., 2015. Mass-balance changes of the debris-covered glaciers in the Langtang Himal, Nepal, from 1974 to 1999. J. Glaciol. 61, 373–386. http://dx.doi.org/10.3189/2015JoG13J237.
Rabus, B., Eineder, M., Roth, A., Bamler, R., 2003. The shuttle radar topography mission—a new class of digital elevation models acquired by spaceborne radar. ISPRS J. Photogramm. Remote Sens. 57, 241–262. http://dx.doi.org/10.1016/S0924-2716(02)00124-7.
Ragettli, S., Bolch, T., Pellicciotti, F., 2016. Heterogeneous glacier thinning patterns over the last 40 years in Langtang Himal, Nepal. Cryosphere 10, 2075–2097. http://dx.doi.org/10.5194/tc-10-2075-2016.
Sakai, A., Nakawo, M., Fujita, K., 1998. Melt rate of ice cliffs on the Lirung Glacier, Nepal Himalayas, 1996. Bull. Glacier Res. 16, 57–66.
Sakai, A., Takeuchi, N., Fujita, K., Nakawo, M., 2000. Role of supraglacial ponds in the ablation process of a debris-covered glacier in the Nepal Himalayas. IAHS Publ. 264, 119–130.
Sakai, A., Nakawo, M., Fujita, K., 2002. Distribution characteristics and energy balance of ice cliffs on debris-covered glaciers, Nepal Himalaya. Arct. Antarct. Alp. Res. 34, 12–19. http://dx.doi.org/10.2307/1552503.
Sakai, A., Fujita, K., Duan, K., Pu, J., Nakawo, M., Yao, T., 2006. Five decades of shrinkage of the July 1st glacier, Qilian mountains, China. J. Glaciol. 52, 11–16. http://dx.doi.org/10.3189/172756506781828836.
Salerno, F., Buraschi, E., Bruccoleri, G., Tartari, G., Smiraglia, C., 2008. Glacier surface-area changes in Sagarmatha national park, Nepal, in the second half of the 20th century, by comparison of historical maps. J. Glaciol. 54, 738–752. http://dx.doi.org/10.3189/002214308786570926.
Scherler, D., Leprince, S., Strecker, M., 2008. Glacier-surface velocities in alpine terrain from optical satellite imagery – accuracy improvement and quality assessment. Remote Sens. Environ. 112, 3806–3819. http://dx.doi.org/10.1016/j.rse.2008.05.018.
Seko, K., 1987. Seasonal variation of altitudinal dependence of precipitation in Langtang Valley, Nepal Himalayas. Bull. Glacier Res. 5, 41–47.
Sugiyama, S., Fukui, K., Fujita, K., Tone, K., Yamaguchi, S., 2013. Changes in ice thickness and flow velocity of Yala Glacier, Langtang Himal, Nepal, from 1982 to 2009. Ann. Glaciol. 54 (64), 157–162. http://dx.doi.org/10.3189/2013AoG64A111.
Surazakov, A., Aizen, V., 2010. Positional accuracy evaluation of declassified Hexagon KH-9 mapping camera imagery. Photogramm. Eng. Remote Sens. 76, 603–608. http://dx.doi.org/10.14358/PERS.76.5.603.
Toutin, T., 2008. ASTER DEMs for geomatic and geoscientific applications: a review. Int. J. Remote Sens. 29, 1855–1875. http://dx.doi.org/10.1080/01431160701408477.
Vincent, C., Wagnon, P., Shea, J.M., Immerzeel, W.W., Kraaijenbrink, P., Shrestha, D., Soruco, A., Arnaud, Y., Brun, F., Berthier, E., Sherpa, S.F., 2016. Reduced melt on debris-covered glaciers: investigations from Changri Nup Glacier, Nepal. Cryosphere 10, 1845–1858. http://dx.doi.org/10.5194/tc-10-1845-2016.
Zhang, Y., Fujita, K., Liu, S., Liu, Q., Nuimura, T., 2011. Distribution of debris thickness and its effect on ice melt at Hailuogou glacier, southeastern Tibetan Plateau, using in situ surveys and ASTER imagery. J. Glaciol. 57, 1147–1157. http://dx.doi.org/10.3189/002214311798843331.